Flooding Waves with Volume of Fluid Method. Experimental Verification

Johannes V. Soulis[1], Athanasios J. Klonidis[2], Dimitrios A. Chrisochoidis[3]

Abstract:--Dam holding back a reservoir of water causes extensive destruction under sudden total collapse. The Navier-Stokes equations were numerically solved for the dam-break phenomenon in lab scale. A set of numerical experiments was performed using the general scientific purposes computational fluid dynamics solver Ansys-Fluent. The position of the free-surface was determined applying the volume of fluid multiphase model. Calculated free-surface elevations and bottom static pressures were compared with available measurements for a converging-diverging flume. The calculations shed light into the flood wave front movement within the flume. The dam-break analysis was enhanced via water depth, static pressure and flow velocities presented in contours and vectors. Aerial nearly top view and a top view clearly depict the front wave tip. Furthermore, the volume of fluid method water volume fraction contour predictions graphics enabled the static pressure experimental data to be directly compared and to derive appropriate conclusions. Satisfactory qualitative and quantitative agreement was observed between current volume of fluid method results and acquired measurements by monitoring the wave front movement for nearly 10.0 s after the sudden and total dam-break collapse. Computational fluid dynamics analysis for the free-surface solution, achieved via volume of fluid method, proved to be a useful tool for dam-break problems.

Index terms--Dam-break, experimental verification, fluent, Volume of fluid method

1 Introduction

THE movement of a 3D flood wave resulting from the breach of a dam has been one of the most important subjects in the rapidly varied unsteady flow from computational point of view. Resulting waves constitute a difficult computational task. When the dam is destroyed, a steep-front wave develops on the downstream side arising from the strong downward released vertical water acceleration of. It is the accurate front wave advancement and its strength that pose problems requiring acceptable engineering solutions.

Ritter [1] gave an analytical solution for the dam-break flood wave water depth and front advancement as early as in 1892. Numerous experimental measurements for the dam-break problem are now widely available [2], [3]. Various 3D codes were applied to unsteady non-hydrostatic flows. Most of them were implemented on fixed grids employing the pressure-velocity decoupling or pressure-linked technique. The computational dam-break flow solution techniques problem can be tackled solving the Reynolds averaged Navier-Stokes equations [4], [5]. The widely used finite-volume Flow-3D code was employed, [6] to simulate supercritical steady flow in gradual expansions proving that computational fluid dynamics models can be powerful tool in engineering analysis and design. Dam-break flood wave measurements conducted over a triangular shape spillway were compared with predictions, [7]. Flood waves depth measurements, [2] resulting from a converging-diverging open channel flume was also tested against predictions using numerical techniques, [8]. Numerical and experimental satisfactory comparison results, [9] were derived of partial-breach dam-break flows using Ansys Fluent. Results were compared with published data on dam-break experiments and simulations carried out by others using shallow water equations modeling.

The general scientific purposes commercially available Fluent software is now widely used for engineering research, development and applications. Validation of the numerical models with experimental available data is always an essential part of acquiring knowledge. The software's strength of volume of fluid (VOF) Fluent code reliability has not yet been widely proven and accepted as a dam-break computational tool. In this area the research is fast advancing [8], [9]. For the current research work the numerical code Ansys-Fluent 14.0, [10], is utilized to verify the computed results, by comparing them with experimental measurements, [2]. The position of the free-surface was determined by applying the VOF multiphase model which is part of the two-phase (water-air) solution technique. Laminar flow is utilized for the Navier-Stokes equation solution since previous research work, [11] showed good agreement between computational results and experimental measurements. Current calculations elucidate, via post processing software, the flood wave front advancement within a converging-diverging flume.

2 Methodology

2.1 Experimental setup

The movement on dry as well as on wet bed of flood waves resulting from total dam-breach was intended to physically model. An effort was made to minimize as possible the 3D

1. *Professor, Fluid Mechanics/Hydraulics Division, Department of Civil Engineering,Democritus University of Thrace, Xanthi, 67100, HELLAS. E-mail: soulis@civil.duth.gr.*
2. *Postdoc Research Assistant, Fluid Mechanics/Hydraulics Division, Department of Civil Engineering,Democritus University of Thrace, Xanthi, 67100, HELLAS. E-mail: klonidis@gmail.com.*
3. *MSc in Hydraulic Engineering, Department of Civil Engineering,Democritus University of Thrace, Xanthi, 67100, HELLAS.*

flow effects by using flat bottom, vertical side walls and mild side wall contractions and expansions. It was intended the flow properties to be invariant in the vertical direction. The resulting testing converging-diverging flume geometry is shown in Fig. 1. Experimental set up details can be found in [2]. The flume has a rectangular cross-section with variable width and was constructed inside the basic research flume of the Hydraulics Laboratory, Civil Engineering Department, Democrition University of Thrace, Hellas. It is a continuous flow circuit permitting bed slopes up to 10.0 ‰. The basic experimental rig is a smooth steel-glass, open-channel flume 21.0 m long, 1.40 m wide and 0.60 m deep. In order to physically model the total dam-breach flow problem it was decided to locate the dam right at the throat flume. Dry and wet bed conditions were applied downstream of the dam. The resulting waves from the instantaneous and com-plete breach of the dam constitute a difficult task for Computational Fluid Dynamicists. When dam is breached, a steep-front wave develops on the downstream side arising from the strong downward ver-tical acceleration of released water. At the same time a depression wave is initiated and travels upstream. At the upstream end of the testing flume a vertical side wall was placed. Thus, a pond was formed each time an experiment was to be carried out. The resulting pond capacity was large enough to sustain continuous unsteady flow for certain time after the dam failure. At the downstream end, free overflow conditions were applied. In cases where an initial depth downstream of the dam was required to be modeled, a variable height weir was used.

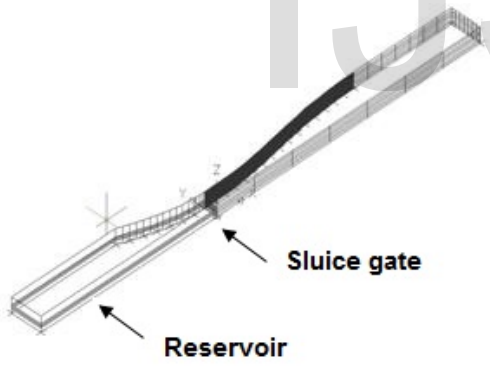

Fig. 1. Converging-diverging flume geometry. Sluice gate is located at throat flume.

2.2 Governing flow equations and boundary conditions

The channel flow is assumed to be 3D, unsteady and viscous, homogeneous, incompressible, with wind and Coriolis forces neglected. In their generality these equations are written as,

$$\frac{\partial(\rho\bar{u})}{\partial t} + \forall(\rho\bar{u}) = 0 \quad (1)$$

$$\frac{\partial(\rho\bar{u})}{\partial t} + \forall(\rho\bar{u}\bar{u}) = -\forall p + \forall\tau + \rho\bar{g} \quad (2)$$

t is the time, ρ is the water density, u is the velocity vector, p is the static pressure, τ is the shear stress and g is the gravity acceleration vector. The water density and molecular viscosity are set to 998.2 (kg/m^3) and 0.001003 (kg/m-s), respectively. The air density and molecular viscosity are set to 1.225 (kg/m^3) and 1.7894×10-5 (kg/m-s), respectively. Laminar flow is considered throughout the flow field. For solid boundary conditions, the no-slip condition is applied. For the free-surface as well as for the down-stream outlet flow, the open boundary condition is applied. Upstream to sluice-gate, the volume of water is specified as being stationary up to the moment of the total sudden rapture. Downstream of the sluice-gate, dry-bed conditions are applied throughout. The use of (2) is consistent with the types of flow developing in channels with smooth bed and walls as considered in the present work. The pressure outlet boundary condition was used for the top surfaces. Atmospheric boundary conditions are applied to top surfaces. As the flooding wave is advancing, air can simultaneously enter the computational domain above the free-surface.

2.3 Volume of fluid method

Current research work utilizes the two-phase (water-air) VOF model approach, [11]. According to this, the volumetric fractions of water and air within each finite-volume are calculated solving the transport equation, excluding the diffusion term,

$$\frac{\partial(\alpha_w)}{\partial t} + \forall(\alpha_w\bar{u}) = 0 \quad (3)$$

with

$$\alpha_w + \alpha_{air} = 1.0 \quad (4)$$

a_w and a_{air} are the volumetric water and air fractions, respectively. As it was noted, within the computational cells, the volume portions of all phases (water-air) sum to unity. The term α_w=1.0 denotes that the under consideration finite-volume is filled with water and α_w=0.0 denotes finite-volume filament with air. Finally, in case where 0.0< α_w <1.0 the finite-volume is located at the edge between free-surface and air. The density and the molecular viscosity are calculated according to,

$$\rho = \alpha_w\rho_w + (1-\alpha_w)\rho_{air} \quad (5)$$

$$\mu = \alpha_w\mu_w + (1-\alpha_w)\mu_{air} \quad (6)$$

ρ_w and ρ_{air} are water and air density respectively, μ_w and μ_{air} are water and air molecular viscosity, respectively. Cells with water in excess of 50.0 % are treated as fully filled with water.

2.4 Computational grid and numerics

Various computational grids were tested for analysis, Table 1. The unstructured mesh is comprised mainly from hexahedra. Current analysis results have been derived using the medium size mesh. The mesh comprises from 273411 cells and 78488 grid nodes. The selection was made for practical and economy related (CPU time) reasons. For the used grid the maximum skewness is 7.31494. The minimum cell volume is 4.54632x10^{-6}

(m^3) while the maximum cell volume is $2.028427x10^{-4}$ (m^3). Fig. 2 shows part of the computational grid utilized for computational analysis. A time step 0.01 s, dictated by Courant criterion, was used to achieve numerical solution. The solution is achieved when all flow physical parameters at each grid node and the continuity equation (inlet-outlet mass flow rate) satisfy the convergence criteria ($<10^{-5}$).

TABLE 1. COMPUTATIONAL GRID NODES

Mesh	Cells	Grid nodes
Dense	467006	126597
Medium	273411	78488
Coarse	138095	47870

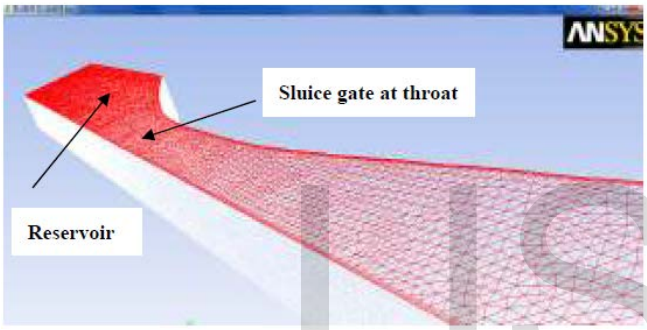

Fig. 2. Computational grid of the converging-diverging flume.

3 RESULTS

3.1 Water depth and static pressure comparison with experimental data at upstream water depth 0.15 m, axial flume distances -8.5 m, +5.0 m and zero slope

Volume of fluid method predictions of the water depth h (m) resulted from dam-break collapse in the converging-diverging open channel flume are compared with measurements at upstream water depth of 0.15 m, axial flume distance -8.5 m and zero slope, fig. 3. Upstream of the sluice gate the water depth is recorded with water height recorders. In this region, for most time duration of the dam-break simulation, the pressure is hydrostatic. Henceforth, the water depth value is identical to static pressure. However, for the downstream to the sluice gate flow region, the flow is non-hydrostatic. In this region the applied pressure transducers record static pressure and the comparison is performed with static pressure predictions. As it was mentioned, the predictions were derived assuming laminar viscous flow. Computational results derived with laminar flow assumption were in good agreement with experimental measurements, [11]. Large amount of turbulence generated from dam-breach has small effects upon the overall flow behavior due to its small time duration.

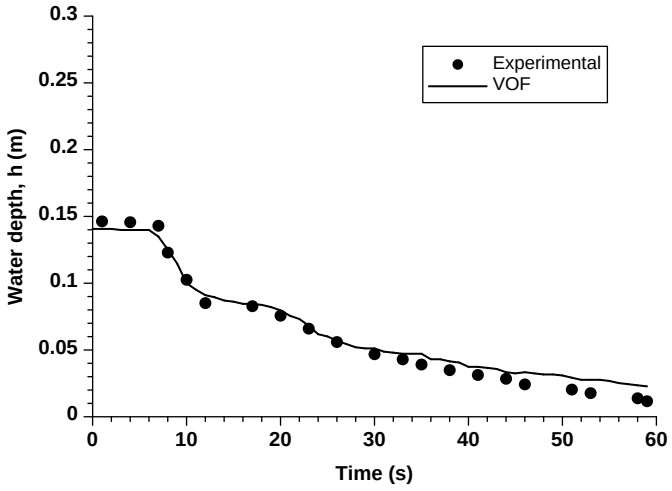

Fig. 3. VOF method water depth h (m) predictions versus experimental data [2] at upstream water depth 0.15 m, axial flume distance -8.5 m and zero slope.

Volume of fluid method predictions of the static pressure head (m) resulted from dam-break collapse in the converging-diverging open channel flume are compared with measurements at upstream water depth of 0.15 m, axial flume distance +5.0 m and zero slope, fig. 4. The comparison is relatively good for the first time instants of the dam-breach. However, after certain time period >40.0 s the comparison worsens.

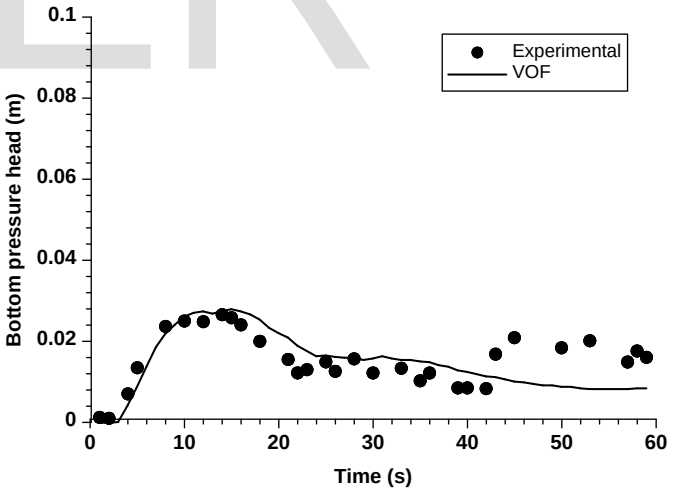

Fig 4. VOF method bottom static pressure head (m) predictions versus experimental data [2] at upstream water depth 0.15 m, axial flume distance +5.0 m and zero slope.

3.2 Water depth and static pressure comparison with experimental data at upstream water depth 0.30 m, axial flume distances -8.5 m, +5.0 m and zero slope.

Volume of fluid method predictions of the water depth h (m) resulted from dam-break collapse in the converging-diverging open channel flume are compared with measurements at upstream water depths of 0.30 m and zero slope, figure 5. The

comparison is considered satisfactory for nearly all time instants.

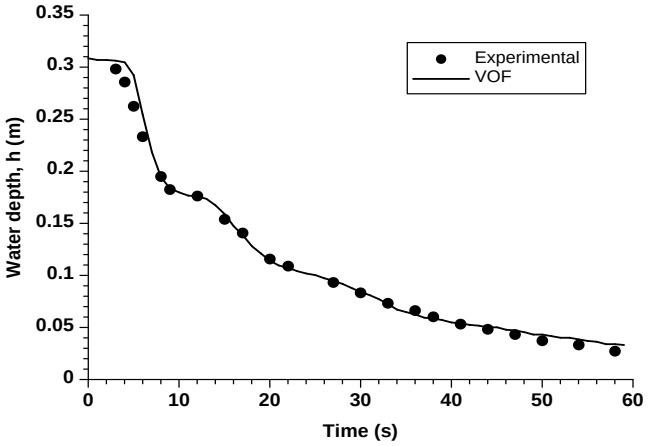

Fig. 5. VOF method water depth h (m) predictions versus experimental data [2] at upstream water depth 0.30 m, axial flume distance -8.5 m and zero slope.

Volume of fluid method predictions of the static pressure head (m) resulted from dam-break collapse in the converging-diverging open channel flume are compared with measurements at upstream water depth of 0.30 m, axial flume distance +5.0 m and zero slope, fig. 6. Here again the comparison is satisfactory for nearly all time instants. This is in contrast to the results shown in fig. 4. This could be attributed to the relatively small water depths developed with 0.15 m initial upstream water depth at this flume location after dam-breach. Discrepancies might be attributed to the measured data than to VOF method predictions.

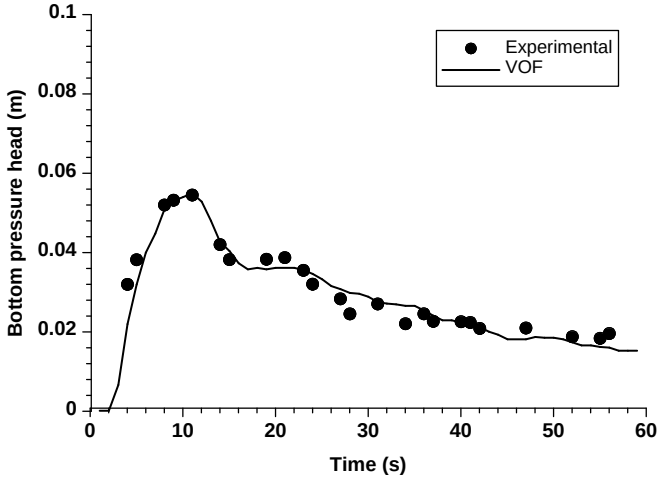

Fig. 6. VOF method bottom static pressure head (m) predictions versus experimental data [2] at upstream water depth 0.30 m, axial flume distance +5.0 m and zero slope.

3.3 Water volume fraction predictions and static pressure experimental data at upstream water depth 0.30 m, zero slope after 2.0 s, 4.0 s and 12.0 s.

Volume of fluid method calculation of water volume fraction at upstream water depth 0.30 m with zero bottom slope after 2.0, 4.0 and 12.0 s is shown in fig. 7. Furthermore, superimposed experimental data for static pressures are also shown

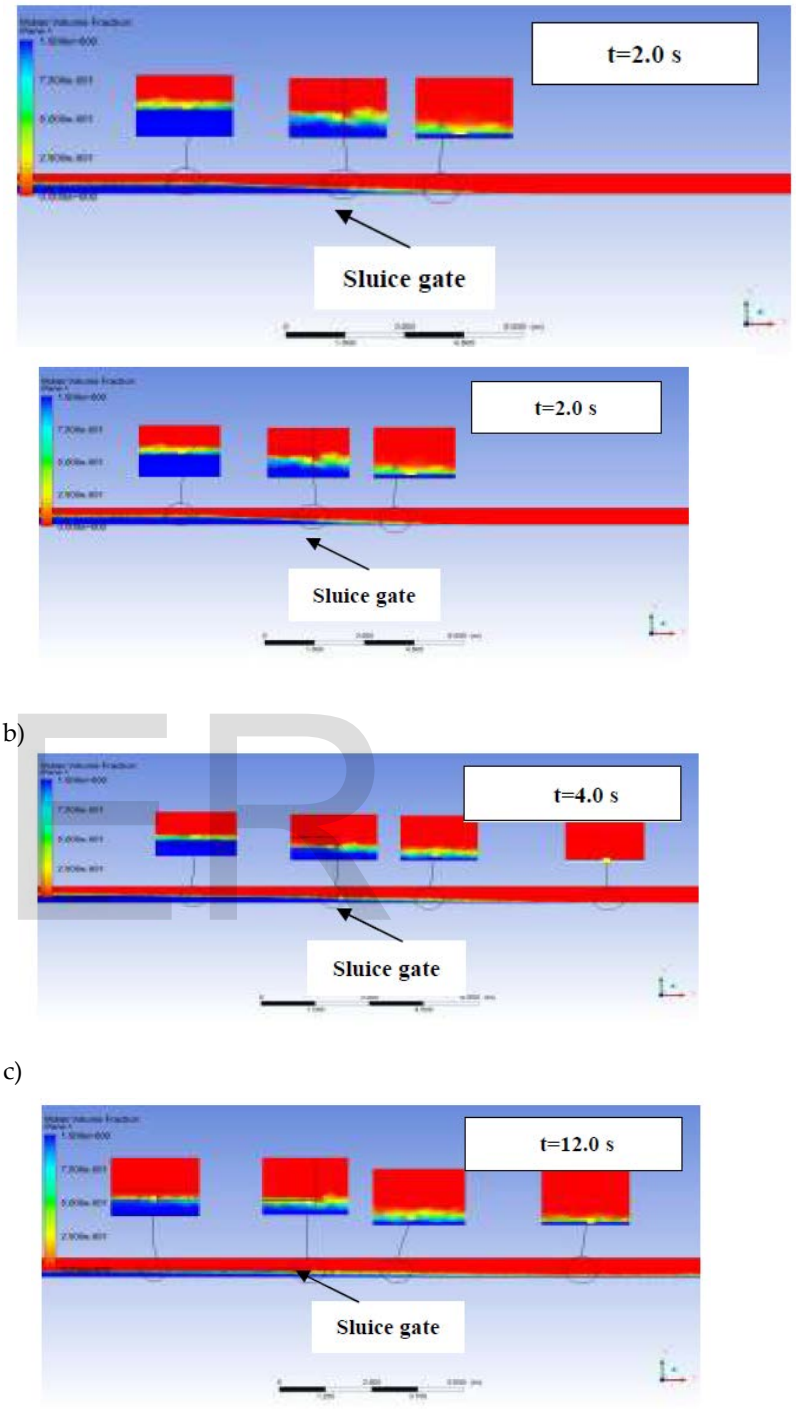

Fig. 7. VOF method water volume fraction predictions and static pressure head (m) experimental data [2] comparison at upstream water depth 0.30 m, zero slope after a) 2.0, b) 4.0 and c) 12.0 s. Cells with water in excess of 50.0 % are treated as fully filled with water. Yellow colored squares indicate experimental data for static pressure. Images shown are side views (flat side).

This is particularly true for the upstream to the sluice gate reservoir flow region. These satisfactory comparisons have already been shown in figures 3 and 5. The sluice gate positioning for each image shown must be noticed. Also, notice

that the images shown in figure 7 are side views (flat side) of the converging-diverging flume.

3.4 Static pressure contours at upstream water depth 0.30 m, zero slopes after 1.0 s, 4.0 s and 10.0 s

The static pressure N/m² contours at upstream water depth 0.30 m with zero bottom slope after 1.0 s, 4.0 s and 10.0 s is shown in fig. 8. As it was noted, the sluice gate is located at the throat of the converging-diverging flume. At remote upstream to the sluice gate flow regions, the static pressure is considered as water depth (hydrostatic). However, at the throat flow region and at further downstream regions the flow is non-hydrostatic. Two views are shown: an aerial nearly top view and a top view. The front movement is clearly depicted in either view. The lowering of the reservoir depth is also clearly shown. The 2D effects of the converging-diverging flume are better depicted in the top view. After 10.0 s flooding, for upstream water depth of 0.15 m test case, the wavefront has nearly reached the very end of the flume (outlet) (not shown). As it is expected the reservoir water depth of 0.30 m results into faster wave front movement and faster lowering of the reservoir water depth in comparison to initial water depth 0.15 m case. After 10.0 s flooding, the wavefront has surpassed the flume outlet.

a)

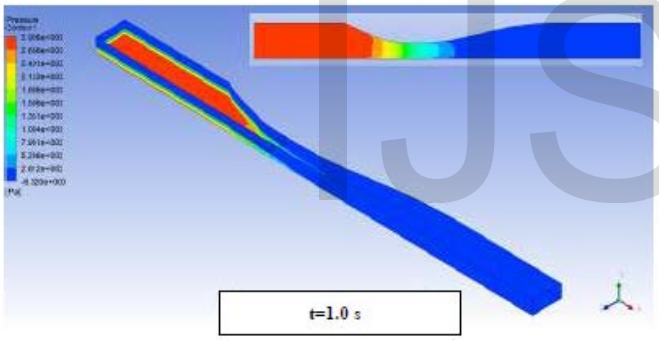

b)

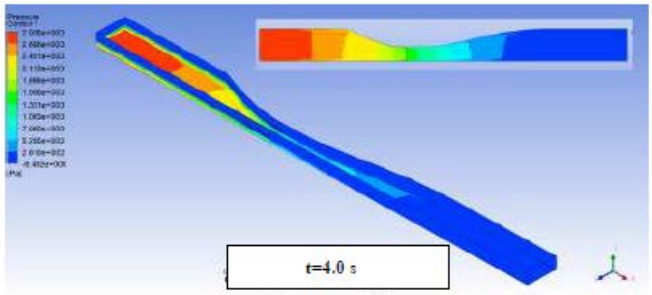

c)

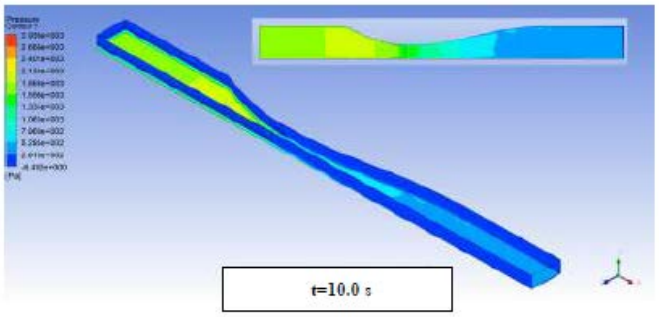

Fig. 8. VOF method static pressure N/m² contour predictions at upstream water depth 0.30 m, zero slope after a) 1.0 s, b) 4.0 s and c) 10.0 s. Two views are shown: an aerial nearly top view and a top view (upper part). The sluice gate is located at throat flume.

3.5 Depth wise velocity magnitude calculation at upstream water depth 0.30 m, zero slope and axial distance +5.0 m after 2.0 s, 5.0 s and 15.0 s

The depth wise magnitude velocity m/s at upstream water depth 0.30 m with zero bottom slope and axial distance +5.0 m after 2.0 s, 5.0 s and 15.0 s is shown in fig. 9. After 2.0 s the wave front has reached the +5.0 m station with max magnitude velocity 1.35 m/s. At 5.0 s the max velocity magnitude keeps the 1.25 m/s velocity magnitude and this value is kept constant for a certain depth wise distance. After 15.0 s the max velocity magnitude has now benn reduced to 0.92 m/s.

a)

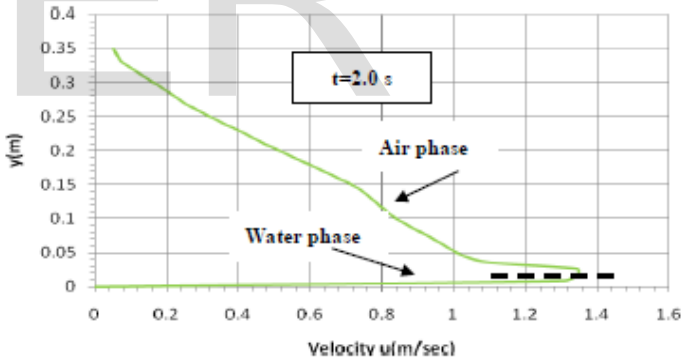

b)

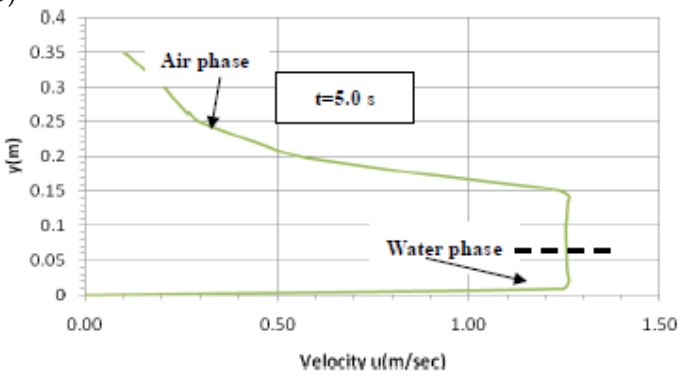

c)

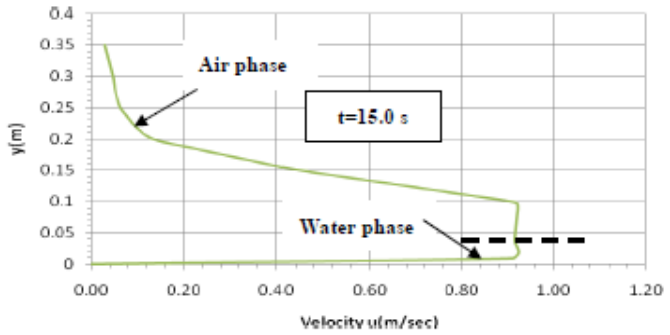

Fig. 9. VOF method depth wise magnitude velocity m/s predictions with upstream water depth 0.30 m, zero slope and axial flume distance +5.0 m from throat after a) 2.0 s, b) 5.0 s and c) 15.0 s. Dotted line separates air from water phase region.

3.6 Velocity magnitude contours at upstream water depth 0.30 m, zero slope after 1.0 s, 4.0 s and 10.0 s

An aerial nearly top view of velocity magnitude m/s vectors at upstream water depth of 0.30 m with zero bottom slope after 1.0 s, 4.0 s and 10.0 s is shown in fig. 10. After 1.0 s from dam-breach, the wave front travels with 2.79 m/s (free-surface). This value is substantially higher to the one appearing with 0.15 m reservoir depth (=1.65 m/s) (not shown). Just upstream to the sluice gate, the velocity is 0.75 m/s. Once the front wave reaches the straight portion of the diverging flume part (after t=4.0 s) it lowers its value to 2.0 m/s. The flow velocity, at the straight portion of the diverging part of the flume, is uniform and gets 1.75 m/s (free-surface) after 10.0 s flooding. The wave front hasn't yet reached the near to inlet flow regions. The front movement is faster than the one corresponding to the 0.15 m upstream reservoir water depth for all instant times shown.

a)

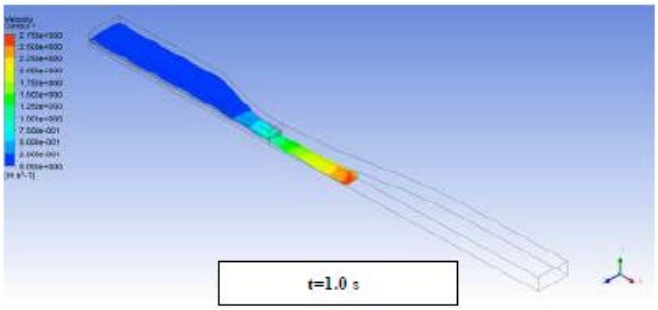

b)

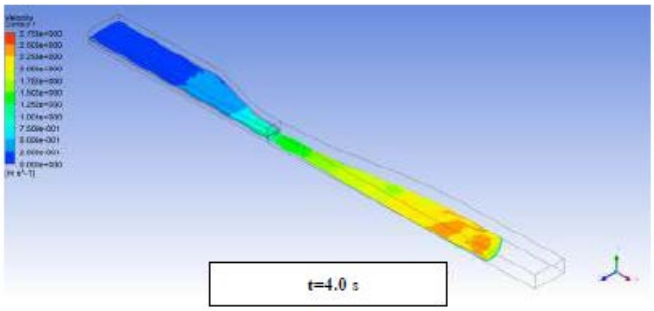

c)

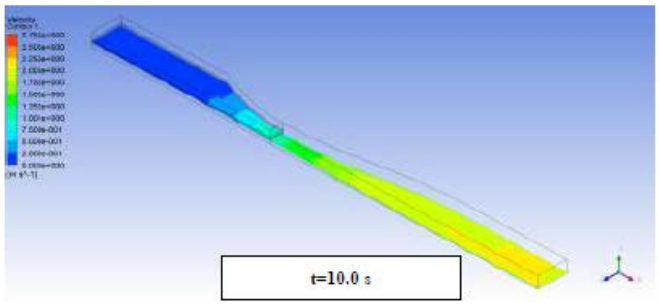

Fig. 10. VOF method velocity magnitude m/s contour predictions at upstream water depth 0.30 m, zero slope after a) 1.0 s, b) 4.0 s and c) 10.0 s; nearly top view. The sluice gate is located at throat flume.

4 Conclusion

The 3D flood wave prediction resulting from dam-breach has been detailed researched via the VOF method. Measurements of water depths and static pressures were available for a converging-diverging flume. These, well documented, measurements are ideally suited for the VOF code validation. Thus, predicted free-surface elevations and bottom static pressures were compared with measurements to examine the applicability of the code.

Water wave impact was also numerically analyzed and compared with experimental data in [13]. In their analysis the applied VOF method yielded good agreement in the initial stages of the problem. However, after certain time period the agreement was deteriorated. Researchers, [5] demonstrated the ability of the VOF method to represent the unsteady flow behavior for the whole observation period. However, they also spotted some differences between experimental data and numerical results.

The currnt method calculations shed light into the flood wave front movement within the flume. The VOF results show relatively good agreement with experimental measurements. This is true for most of the time after dam-breach. Particularly good agreement occurs at the upstream to the sluice gate flow region. Between predictions and experimental measurements there are some disagreements in the water tip location. These disagreements are pronounced at remote downstream of the sluice gate flow regions where the water depth is low. More research work is needed for the viscosity model closing.

The usage the VOF method for the dam-break analysis enabled the elucidation and the proper visualization of the whole unsteady flow process. Static pressure and velocity magnitude contours shown in aerial nearly top view and a top view clearly depict the front wave tip. Furthermore, the VOF method graphics for water volume fraction contours enabled the static pressure experimental data to be directly compared and to derive appropriate conclusions.

References

[1] A. Ritter, "Die Fortplanzung der Wasserwellen, Zeitschrift des Vereines Deutscher Ingeniere", Vol. 36, no. 33, pp. 947-954, 1892

[2] C.V. Bellos, J.V. Soulis and Sakkas, J.G., "Experimental

Investigation of Two-dimensional Dam-break Induced Flows", *Journal of Hydraulic Research*, Vol 30 no. 1, pp. 47-63, 1992

[3] R. Aleixo, B. Spinewine, S. Soares-Frazão and Y. Zech, "Non-intrusive Measurements of Water Surface and Velocity Profiles in a Dam-break Flow", *33rd IAHR Congress: Water Engineering for a Sustainable Environment*, Vancouver, British Columbia, pp. 6898-6905, 2009

[4] A. Georgoulas, A. Pandremmenou and V. Hrissanthou, "3D Dam-break Numerical Modeling", *International Conference of Protection and Restoration of the Environment XI*. Thessaloniki, Greece, 2012

[5] C. Biscarini, S.D. Francesco, and P. Manciola, "CFD Modeling Approach for Dam-break Flow Studies", *Hydrology and Earth System Sciences*, Vol. 14, pp. 705-718, 2010

[6] A.I. Stamou, D.G. Chapsas and G.C. Christodoulou, "3D Numerical Modeling of Super-critical Flow in Gradual Expansions", *Journal of Hydraulic Research*, Vol. 46, pp. 402-409, 2008

[7] S. Soares-Frazao, C. de Bueger , V. Dourson and Y. Zech, "Experiments of Dam-break Wave over a Triangular Bottom Sill", *Journal of Hydraulic Research*, Vol. 25, pp. 73-86, 2007

[8] V. Bellos and V. Hrissanthou, "Numerical Simulation of a Dam-break Wave", *European Water*, 7/8, pp. 3-15, 2011.

[9] L. A. Larocque, "Experimental and numerical modeling of dam-break and levee-breach flows", Ph.D. Thesis, University of South Carolina, 135 pages, Publication number 3548847, 2012

[10] Ansys Inc., "Ansys Fluent Theory Guide", Release 14.0, 2012

[11] T.U.L. Liyanage, G.A. Kikkert and C. Shang, "Numerical Simulation of Dam-break Generated Flow into a Storm Drain", *Proc of the 7th International Conference on Asian and Pacific Coasts (APAC 2013)* Bali, Indonesia, September 24-26, 2013

[12] K. Abdolmaleki, K.P. Thiagarajan and M.T. Morris-Thomas, "Simulation of the Dam-break Problem and Impact Flows using a Navier-Stokes Solver", *15th Australasian Fluid MUchanics Conference*, The University of Sydney, Sydney, Australia, 2004

[13] P.G. Panickera, A. Goelb and H.R. Iyerc, "Numerical Modeling of Advancing Wave Front in Dam-break Problem by Incompressible Navier-Stokes Solver", *International Conference on Water Resources, Coastal and Ocean Engineering (ICWRCOE 2015)*, Aquatic Procedia 4 (2015), pp. 861–867, 2214-241X, 2015